JACS JOURNAL OF THE AMERICAN CHEMICAL SOCIETY

Article

Cite This: J. Am. Chem. Soc. 2019, 141, 17854−17860

pubs.acs.org/JACS

# $ReB_6^-$: A Metallaboron Analog of Metallabenzenes

Ling Fung Cheung, Joseph Czekner, G. Stephen Kocheril, and Lai-Sheng Wang*

Department of Chemistry, Brown University, Providence, Rhode Island 02912, United States

Supporting Information

**ABSTRACT:** Metallabenzenes are a class of molecules in which a CH unit in benzene is replaced by a functionalized transition-metal atom. While all-boron analogues of aromatic and antiaromatic hydrocarbons are well-known, there have not been any metallaboron analogs. We have produced and investigated two metal-doped boron clusters, $ReB_6^-$ and $AlB_6^-$, using high-resolution photoelectron imaging and quantum chemical calculations. Vibrationally resolved photoelectron spectra have been obtained and compared with the theoretical results. The $ReB_6^-$ cluster is found to be perfectly planar with a B-centered hexagonal structure ($C_{2v}$, $^1A_1$), while $AlB_6^-$ is known to have a similar structure, but with a slightly out-of-plane distortion ($C_s$, $^1A'$). Chemical bonding analyses show that the closed-shell $ReB_6^-$ is doubly $\sigma$- and $\pi$-aromatic, while $AlB_6^-$ is known to be $\sigma$-aromatic and $\pi$-antiaromatic. The out-of-plane distortion in $AlB_6^-$ is due to antiaromaticity, akin to the out-of-plane distortion of the prototypical antiaromatic cyclooctatetraene. The $\pi$-bonding in $ReB_6^-$ is compared with that in both benzene and rhenabenzene $[(CO)_4ReC_5H_5]$, and remarkable similarities are found. Hence, $ReB_6^-$ can be viewed as the first metallaboron analog of metallabenzenes and it may be viable for syntheses with suitable ligands.

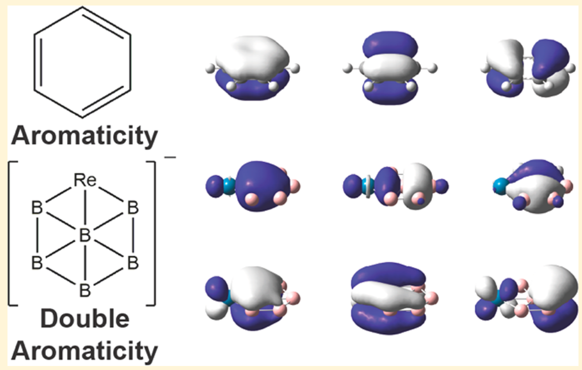




## INTRODUCTION

Metallabenzenes consist of an interesting class of organometallic compounds, in which one CH group in benzene is substituted by a metal atom.[1−4] Various metallabenzenes have been synthesized,[5−12] including several recently reported rhenabenzenes.[13,14] Interesting aromatic and organometallic properties have been found for metallabenzenes.[2,3,15,16] Both planar and nonplanar metallabenzenes have been observed. It was suggested that not only electronic but also steric factors can play a role in the planarity of metallabenzenes.[17,18] Recently, a strong correlation between the calculated energy of the highest occupied $\sigma$-type molecular orbital and the planarity of different metallabenzenes has been shown, resulting in the suggestion of the so-called "$\sigma$-control mechanism" for the nonplanarity of metallabenzenes.[18]

Boron is known to form delocalized bonds due to its electron deficiency.[19] While borane cages ($B_nH_n^{2-}$), in particular, $B_{12}H_{12}^{2-}$, have long been considered as three-dimensional aromatic systems,[20−23] the aromaticity and planarity of size-selected bare boron clusters have been established fairly recently,[24−31] via extensive joint experimental and theoretical investigations.[32−39] The study of size-selected boron clusters has given rise to the concepts of $\sigma$- and $\pi$-aromaticity, antiaromaticity, and even conflicting aromaticity, which can be described well by the adaptive natural density partitioning (AdNDP) method.[40] Similar to metallabenzenes, both electronic and steric factors can play a role in the planarity of aromatic boron clusters. For example, the $B_{12}$ cluster is aromatic with six $\pi$-electrons, but it features an out-of-plane distortion ($C_{3v}$) because the $B_9$ ring is too small to host a $B_3$ unit.[24] A subsequent study showed that substitution of a peripheral B atom by a larger, isoelectronic Al atom leads to a perfect planar and aromatic $AlB_{11}$ cluster.[41] On the other hand, substitution of a B atom in the hexagonal $C_{2v}$ $B_7^-$ cluster[34] led to a $C_s$ $AlB_6^-$ cluster, which has a planar $B_6^-$ moiety with the peripheral Al atom slightly out of plane because it has conflicting aromaticity: the $AlB_6^-$ cluster is $\sigma$-aromatic, but $\pi$-antiaromatic with four $\pi$-electrons.[41] An interesting question arises: can the Al atom be replaced in $AlB_6^-$ by a transition-metal atom to produce a perfectly planar and aromatic hexagonal $MB_6^-$ cluster, which would be a metallaboron analog of metallabenzenes?

In addition to the Al-substituted $B_7^-$, a number of $MB_6^-$-type clusters have been studied, including main group, lanthanide, and transition-metal substituents.[42−50] The early reports of the aromatic $D_{6h}$ $CB_6^{2-}$ and the associated $D_{7h}$ $CB_7^-$ species were unfortunately higher-energy isomers,[42,43] and their global minima were found by joint potential energy surface and theoretical studies to feature less symmetric structures in which the C atom is located on the periphery of the clusters.[45,46] The gold atom in $AuB_6^-$ is found to bond to the $B_6$ moiety via a single covalent bond akin to a H atom.[47] The $SmB_6^-$ and $CeB_6^-$ clusters have been reported recently,[49,50] both exhibiting planar structures similar to that of $AlB_6^-$, but $SmB_6^-$ was found to be doubly antiaromatic. The

**Received:** August 22, 2019
**Published:** October 15, 2019





DOI: 10.1021/jacs.9b09110
J. Am. Chem. Soc. 2019, 141, 17854−17860

$TaB_6^-$ cluster was found to have a perfect planar structure and was considered to be doubly aromatic.[48] However, it has a triplet ground state ($C_{2v}$, $^3B_1$) with five delocalized $\pi$-electrons and a single nonbonding 5d-electron. Hence, a planar $MB_6^-$ metallaboron cluster with similar electronic structure as benzene or metallabenzenes has not been reported.

In the current study, we investigate the $ReB_6^-$ cluster using high-resolution photoelectron (PE) imaging with complete vibrational resolution and quantum chemical calculations. The $AlB_6^-$ cluster is revisited using high-resolution PE imaging as a comparison. A more accurate electron affinity (EA) is measured for $AlB_6$, and the vibrationally resolved PE spectra confirm the previously reported bent structure for $AlB_6^-$.[41] The structure distortion in $AlB_6^-$ is consistent with its $\pi$-antiaromaticity, analogous to the out-of-plane distortion in the cyclooctatetraene ($C_8H_8$). The $ReB_6^-$ cluster is found to be closed-shell and perfectly planar. Chemical bonding analyses reveal that $ReB_6^-$ possesses six delocalized $\sigma$-electrons and six delocalized $\pi$-electrons, consistent with double aromaticity. The $\pi$-bonding in $ReB_6^-$ is found to display remarkable similarities to that in benzene and the recently synthesized rhenabenzenes.

## ■ EXPERIMENTAL AND THEORETICAL METHODS

**High-Resolution Photoelectron Imaging.** The experiments were conducted using a high-resolution PE imaging system coupled to a laser vaporization cluster source, which was described in detail previously.[51] Briefly, the $ReB_6^-$ and $AlB_6^-$ clusters were produced by focusing the second harmonic of a Nd:YAG laser onto a disk target. The target was made of a mixture of enriched $^{10}B$, Re, and Ag powders for the production of $ReB_6^-$ or of enriched $^{11}B$, Al, and Ag powders for that of $AlB_6^-$ (the Ag powder was added as a binder). The laser-induced plasma formed inside the nozzle was quenched by a helium carrier gas seeded with 10% argon, which initiated the nucleation. The nascent clusters were entrained in the carrier gas and underwent a supersonic expansion to produce a cold cluster beam. Anionic clusters were extracted perpendicularly into a time-of-flight mass spectrometer. The $^{187}Re^{10}B_6^-$ or $Al^{11}B_6^-$ clusters of interest were mass-selected before entering the interaction zone of the velocity-map imaging (VMI) system.

A Deyang Tech dye laser pumped by a Nd:YAG laser was used to detach electrons from the size-selected clusters. Photoelectrons were focused onto a set of microchannel plates coupled with a phosphor screen and a charge-coupled device camera. Each experiment at a given photon energy required about 100 000−200 000 laser shots to achieve reasonable signal-to-noise ratios. The VMI lens was calibrated using the photoelectron images of $Au^-$ at various photon energies. The photoelectron images were analyzed using the maximum entropy method (MEVIR and MEVELER).[52] The typical energy resolution of the VMI system was ~0.6% for high kinetic energy electrons and could be as good as 1.2 $cm^{-1}$ for low kinetic energy electrons.[51]

**Theoretical Method.** We carried out global minimum searches for $ReB_6^-$ using the simulated annealing algorithm coupled with density functional theory (DFT) for geometry optimization.[53−56] Around 300 different structures were generated and optimized at the PBE/LAN2DZ level of theory.[57,58] The low-lying isomers within 1 eV of the global minima were further optimized using the B3LYP functional with the aug-cc-pVTZ-pp basis set and the ECP60MDF relativistic effective core potential (ECP) for Re and the aug-cc-pVTZ basis set for B.[59−61] Geometric optimization and vibrational analyses were carried out for $ReB_6^{-/0}$. Since the global minima of $AlB_6^{-/0}$ were already known,[41] we redid the geometric optimization and performed vibrational analyses at the B3LYP/aug-cc-pVTZ level of theory.[59,62] For comparison, we optimized the structures of benzene and a symmetric model of rhenabenzene [$(CO)_4ReC_5H_5$] at the B3LYP/aug-cc-pVTZ/Re/aug-cc-pVTZ-pp level of theory and performed chemical bonding analyses.

The adiabatic detachment energy (ADE) for the ground-state transition, which also represents the EA of the neutral, was calculated as the energy difference between the optimized anion and its corresponding neutral. Coupled cluster calculations [CCSD(T)] were done on the B3LYP geometry for $ReB_6^{-/0}$ using the same basis sets and ECP to calculate the ADE. Chemical bonding analyses were done using the AdNDP method.[40] Nucleus-independent chemical shift (NICS)[63] calculations were carried out to examine the aromaticity of $ReB_6^-$. Franck−Condon simulations were performed using PESCAL.[64] All calculations were done using Gaussian 09.[65]

## ■ RESULTS

**Experimental Results.** The PE images and spectra of $ReB_6^-$ at six different photon energies are shown in Figure 1. A sharp peak labeled as $X$ denotes the 0−0 transition, which is from the anion ground state to that of the neutral. The $X$ peak defines the EA of $ReB_6^-$ to be 2.3478 ± 0.0008 eV. Extremely weak intensities were observed for transitions to vibrationally excited states, indicating very little geometry change upon photodetachment. Discernable vibrational peaks are labeled as $a$−$g$ and their binding energies and assignments (vide infra) are summarized in Table 1.

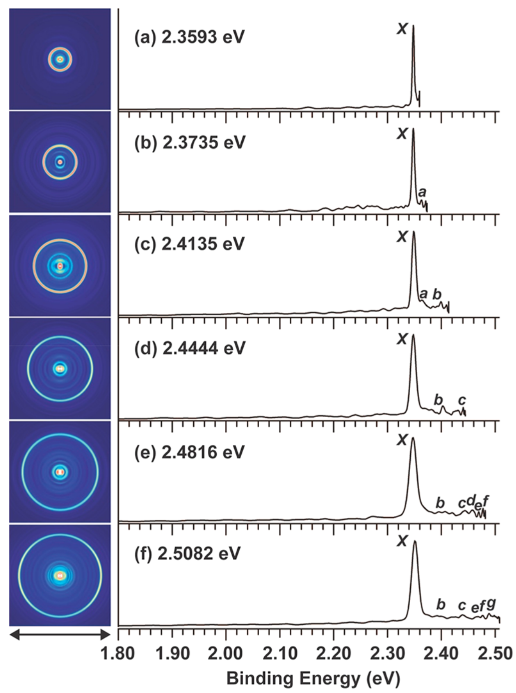


**Figure 1.** Photoelectron images and spectra of $ReB_6^-$ at different photon energies. The double arrows below the images denote the laser polarization.

The PE spectra of $AlB_6^-$ were reported previously at three photon energies (193, 266, and 355 nm), which revealed numerous detachment transitions.[41] The 355 nm spectrum was partially vibrationally resolved for the ground-state transition, yielding an average vibrational spacing of 480 ± 40 $cm^{-1}$ and an EA of 2.49 ± 0.03 eV for $AlB_6$. Figure 2 shows the PE images and high-resolution PE spectra for the ground-state transition of $AlB_6^-$ at various photon energies. Much more complicated vibrational structures are resolved, suggesting significant structural changes between the ground states of the $AlB_6^-$ anion and its neutral. The sharp peak labeled $X$ in Figure 2a denotes the 0−0 transition and yields a more accurate EA of 2.4958 ± 0.0004 eV for $AlB_6$. The resolved vibrational peaks


DOI: 10.1021/jacs.9b09110
J. Am. Chem. Soc. 2019, 141, 17854−17860

**Table 1. Measured Binding Energies (BE), Energy Shifts Relative to the 0−0 Transition, and Assignments of the Observed Vibrational Peaks in the PE Spectra of $ReB_6^-$ and Comparison with the Computed Vibrational Frequencies of $ReB_6$ at the B3LYP/aug-cc-pVTZ/Re/aug-cc-pVTZ-pp Level of Theory**

| | experimental | | | | |
|---|---|---|---|---|---|
| peak | BE (eV) | assignment | symm | energy shift ($cm^{-1}$) | theoretical[a] frequency ($cm^{-1}$) |
| *X* | 2.3478(8) | | | | |
| *a* | 2.3627(14) | $10_0^1$ | $b_1$ | 120(9) | 137 |
| *b* | 2.3989(31) | $6_0^1$ | $a_1$ | 412(18) | 431 |
| *c* | 2.4401(25) | $4_0^1$ | $a_1$ | 744(15) | 761 |
| *d* | 2.4574(37) | $4_0^1 10_0^1$ | $b_1$ | 884(22) | 898 |
| *e* | 2.4693(17) | $3_0^1$ | $a_1$ | 980(11) | 919 |
| *f* | 2.4770(7) | $2_0^1$ | $a_1$ | 1042(6) | 1080 |
| *g* | 2.4889(18) | $1_0^1$ | $a_1$ | 1138(11) | 1184 |

[a]The calculated ADE for $ReB_6^-$ is 2.05 eV at the B3LYP/aug-cc-pVTZ/Re/aug-cc-pVTZ-pp level and 2.42 eV at the CCSD(T)/aug-cc-pVTZ/Re/aug-cc-pVTZ-pp level of theory.

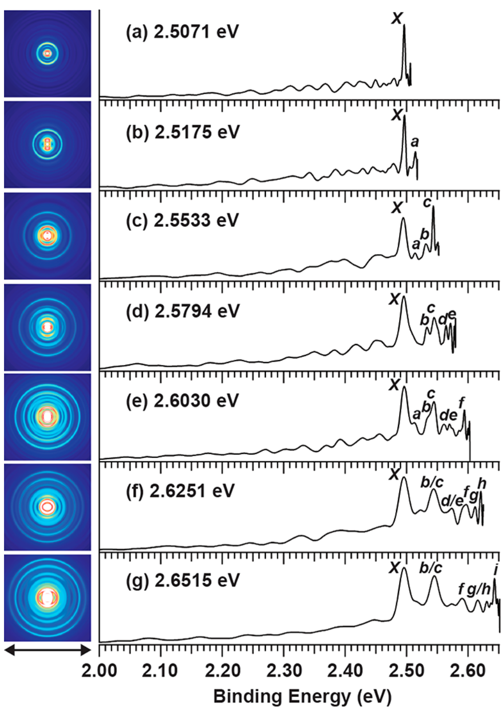


**Figure 2.** Photoelectron images and spectra of $AlB_6^-$ at different photon energies. The double arrows below the images denote the laser polarization.

are labeled as *a*−*i* and their binding energies and assignments are summarized in Table 2. Several peaks are assigned to fundamental vibrational excitations (*a*−*c*, *e*, and *h*), while the others are assigned to overtones (*f* and *g*) or a combination vibrational level (*d*) (vide infra).

**Computational Results.** The global minimum of $ReB_6^-$ was found to be a B-centered six-membered ring with a peripheral Re atom, similar to that of $AlB_6^-$, except that $ReB_6^-$ is perfectly planar with $C_{2v}$ symmetry (Figure 3a). The anion has a closed-shell electron configuration ($^1A_1$): $1a_1^2 1b_2^2 2a_1^2 2b_2^2 3a_1^2 1b_1^2 4a_1^2 3b_2^2 5a_1^2 4b_2^2 1a_2^2 2b_1^2 6a_1^2$. The valence molecular orbital (MO) pictures are displayed in Figure S1a of the Supporting Information (SI). The $6a_1$ highest

**Table 2. Measured Binding Energies (BE), Energy Shifts Relative to the 0−0 Transition, and Assignments of the Observed Vibrational Peaks in the PE Spectra of $AlB_6^-$ and Comparison with the Computed Vibrational Frequencies of $AlB_6$ at the B3LYP/aug-cc-pVTZ Level of Theory**

| | experimental | | | | |
|---|---|---|---|---|---|
| peak | BE (eV) | assignment | symm | energy shift ($cm^{-1}$) | theoretical[a] frequency ($cm^{-1}$) |
| *X* | 2.4958(4) | | | | |
| *a* | 2.5140(9) | $9_0^1$ | a′ | 147(5) | 162 |
| *b* | 2.5322(5) | $8_0^1$ | a′ | 294(4) | 362 |
| *c* | 2.5432(11) | $7_0^1$ | a′ | 382(7) | 396 |
| *d* | 2.5638(21) | $7_0^1 9_0^1$ | a′ | 548(12) | 558 |
| *e* | 2.5713(6) | $5_0^1$ | a′ | 609(4) | 618 |
| *f* | 2.5935(29) | $7_0^2$ | a′ | 788(16) | 792 |
| *g* | 2.6107(35) | $14_0^2$ | a′ | 927(20) | 892 |
| *h* | 2.6206(15) | $2_0^1$ | a′ | 1007(9) | 992 |
| *i* | 2.6428(10) | $7_0^3$ | a′ | 1186(6) | 1188 |

[a]The calculated ADE for $AlB_6^-$ is 2.21 eV at the B3LYP/aug-cc-pVTZ level and 2.45 eV at CCSD(T)/aug-cc-pVTZ level of theory.

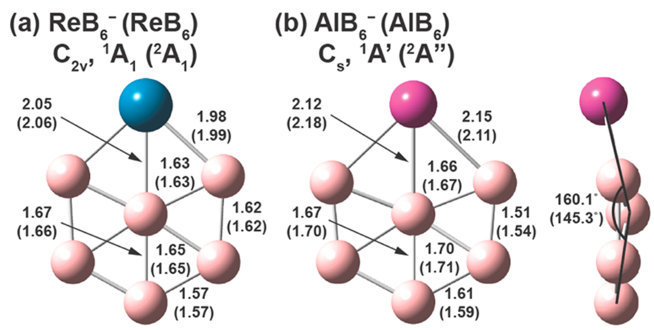


**Figure 3.** Optimized structures of (a) $ReB_6^-$ and $ReB_6$ (in parentheses) and (b) $AlB_6^-$ and $AlB_6$ (in parentheses). Bond lengths are given in angstroms and the dihedral angles in $AlB_6^{-/0}$ are in degrees. The point group symmetries and electronic states are also given.

occupied MO (HOMO) is comprised of the nonbonding $5d_{z^2}$ orbital. Removal of one electron from the HOMO of $ReB_6^-$ gives rise to the $^2A_1$ neutral ground state. Very little geometry change is observed between the anion and the neutral ground states due to the nonbonding nature of the HOMO, in agreement with the observed PE spectra (Figure 1). It has been shown previously that carbon avoided the central position of a $B_6$ ring in the $CB_6^-$ cluster because carbon is more electronegative and prefers to form localized bonds on the periphery of the planar $CB_6^-$ cluster.[46] In the current case of $ReB_6^-$, the Re atom is too large to fit in the center of a $B_6$ ring. There are both geometric and electronic criteria to form $M©B_n^-$-type metal-centered aromatic borometallic clusters.[66−68] Recently, both $ReB_8^-$ and $ReB_9^-$ are found to be new members of the transition-metal-centered borometallic molecular wheel family.[69]

The optimized geometry of the $AlB_6^-$ anion and its corresponding neutral are shown in Figure 3b. As reported previously,[41] $AlB_6^-$ is a B-centered six-membered ring with a slight out-of-plane distortion by the Al atom (Figure 3b). The planar $C_{2v}$ structure possesses an imaginary frequency and is 0.05 kcal/mol higher in energy than the distorted $C_s$ structure. Further optimization following the imaginary frequency leads to the bent global minimum, which is closed-shell with $C_s$


DOI: 10.1021/jacs.9b09110
J. Am. Chem. Soc. 2019, 141, 17854−17860

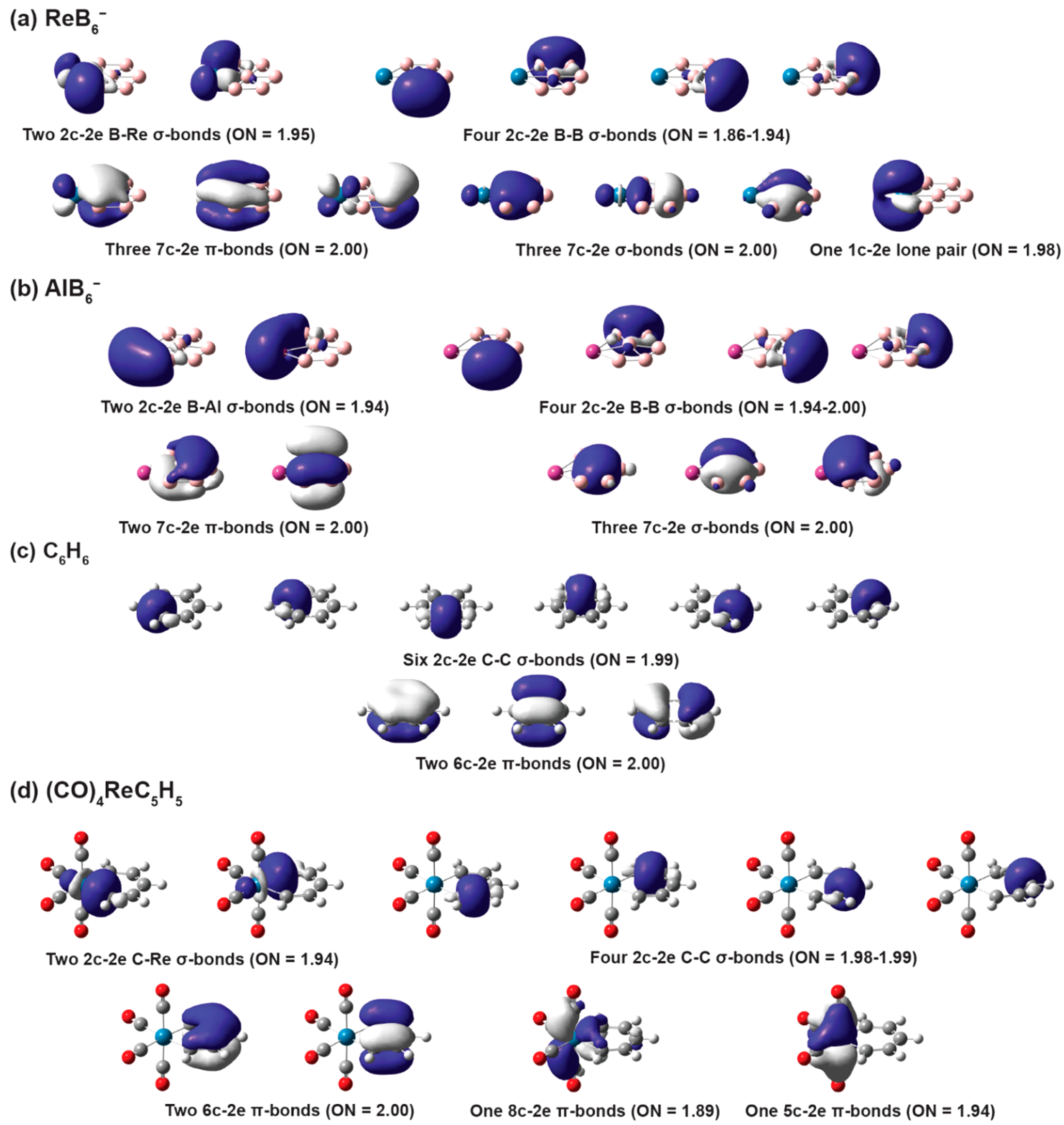


**Figure 4.** AdNDP analyses for (a) $ReB_6^-$, (b) $AlB_6^-$, (c) benzene, and (d) $(CO)_4ReC_5H_5$. For simplicity, only bonds related to the C atoms in benzene and the atoms in the six-member ring of rhenabenzene are shown.

symmetry ($^1A'$). The valence MO pictures of $AlB_6^-$ are shown in Figure S1b (SI) and its HOMO is a $\pi$-bonding orbital. Removal of an electron from the HOMO of $AlB_6^-$ yields the ground state of the neutral ($^2A''$) with the same symmetry but a much larger out-of-plane distortion by the Al atom. The large geometry change between the anion and neutral ground state is consistent with the complicated vibrational structures observed in the high-resolution PE spectra of $AlB_6^-$ (Figure 2).

## ■ DISCUSSION

**Comparison of the High-Resolution Photoelectron Spectra of $ReB_6^-$ with the Theoretical Results.** The calculated ADE of 2.42 eV for $ReB_6^-$ at the CCSD(T) level agrees well with the experimental value of 2.3478 eV (Table 1). To help assign the observed weak vibrational features, we computed the vibrational frequencies for both the $ReB_6^-$ anion and its neutral, as given in Table S1 (SI). We also did a Franck−Condon simulation as exhibited in Figure S2a (SI), which shows almost negligible Franck−Condon factors for any vibrational excitations accompanying the photodetachment process, because of the small geometry changes between the anion and neutral (Figure 3a). The only discernible Franck−Condon factor is for mode $\nu_4$, corresponding to peak *c* (Table 1). The other mode with visible Franck−Condon factor is the $\nu_1$ mode, corresponding to peak *g*. The displacement vectors of these modes are shown in Figure S3a (SI), which are consistent with the minor geometry changes between the anion and neutral (Figure 3a). Peaks *b*, *e*, and *f* can also be assigned to three totally symmetric fundamental vibrational modes, $\nu_6$, $\nu_3$, and $\nu_2$, respectively, as shown in Table 1. Peak *a* is assigned to a symmetry-forbidden mode, $\nu_{10}$, which corresponds to the lowest-frequency out-of-plane bending mode (Figure S3a, SI). We have previously observed symmetry-forbidden vibrational modes, also corresponding to low-frequency bending modes.[70] Similarly, peak *d* can be tentatively assigned to a combinational mode of $\nu_{10}$ and $\nu_4$. Overall, the observed vibrational features agree well with the computed frequencies and the Franck−Condon simulation,


DOI: 10.1021/jacs.9b09110
J. Am. Chem. Soc. 2019, 141, 17854−17860

confirming unequivocally the $C_{2v}$ planar global minimum structures for $ReB_6^-$ and neutral $ReB_6$ (Figure 3a).

**Comparison of the High-Resolution Photoelectron Spectra of $AlB_6^-$ with the Theoretical Results.** The more accurate ADE of 2.4958 eV measured for $AlB_6^-$ agrees well with the calculated value of 2.45 eV at the CCSD(T)/aug-cc-pVTZ level of theory (Table 2). Much more complicated vibrational structures are resolved in the high-resolution PE spectra of $AlB_6^-$ (Figure 2), because of the large geometry changes between the anion and the neutral (Figure 3b). The calculated vibrational frequencies (Table S2, SI) and the Franck−Condon simulation (Figure S2b, SI) are used to guide the vibrational assignments. The large out-of-plane distortion of the Al atom in the neutral (Figure 3b) suggests that the most Franck−Condon-active vibrational mode should be the Al-bending mode during photodetachment. This is the $\nu_7$ mode with a computed frequency of 396 $cm^{-1}$ (Figure S3b, SI), corresponding to the strongest vibrational peak *c* in the PE spectra (Figure 2), which gives an experimental frequency of 395 $cm^{-1}$. Peaks *f* and *i* also belong to the $\nu_7$ vibrational progression, as shown in Table 2. Peaks *a*, *b*, *e*, and *h* can be assigned to four more fundamental vibrational frequencies, as given in Table 2. Finally, peak *d* is assigned to a combinational mode of $\nu_7$ and $\nu_9$, and peak *g* is assigned to the overtone of mode $\nu_{14}$ (Table 2). The displacement vectors for all the observed vibrational modes of $AlB_6$ are shown in Figure S3b (SI). Overall, the Franck−Condon simulation and the computed vibrational frequencies are in excellent agreement with the high-resolution photoelectron spectra, confirming the bent structure of $AlB_6^-$ and the large geometry changes in the neutral relative to the anion (Figure 3b).

**Bonding Analyses for $ReB_6^-$ and $AlB_6^-$.** We performed chemical bonding analyses for $ReB_6^-$ and $AlB_6^-$ using the AdNDP method.[40] The AdNDP results for $ReB_6^-$ and $AlB_6^-$ are compared with those of benzene and rhenabenzene in Figure 4. The AdNDP analyses for $ReB_6^-$ and $AlB_6^-$ reveal six two-center two-electron (2c−2e) peripheral B−B/B−Re bonds, a $5d_{z^2}$ lone pair, and six delocalized bonds for $ReB_6^-$ (Figure 4a) and six 2c−2e peripheral B−B/B−Al bonds and five delocalized bonds for $AlB_6^-$ (Figure 4b). The $ReB_6^-$ cluster features three totally delocalized 7c−2e $\sigma$-bonds and three totally delocalized 7c−2e $\pi$-bonds (Figure 4a), both fulfilling the $4n + 2$ Hückel rule for aromaticity, rendering $ReB_6^-$ doubly aromatic. The AdNDP analyses for $AlB_6^-$ have been reported previously[41] and are presented here for comparison. As shown in Figure 4b, $AlB_6^-$ contains three totally delocalized 7c−2e $\sigma$-bonds and two totally delocalized 7c−2e $\pi$-bonds, which render $AlB_6^-$ $\sigma$-aromatic and $\pi$-antiaromatic. Hence, $AlB_6^-$ provides a rare case of conflicting aromaticity. The $\pi$-antiaromaticity in $AlB_6^-$ explains its out-of-plane distortion, analogous to the out-of-plane distortion of the prototypical antiaromatic cyclooctatetraene ($C_8H_8$).

**Comparison of the Delocalized $\pi$-Bonds and Aromaticity in $ReB_6^-$ with Those in Benzene and Rhenabenzene.** We also conducted AdNDP analyses for benzene and [$(CO)_4ReC_5H_5$] for comparison, as shown in parts c and d of Figure 4, respectively. We see that the three delocalized $\pi$-bonds in $ReB_6^-$ are similar to those in benzene, with the 5d orbitals participating in the delocalized bonding. Curiously, the two 6c−2e delocalized $\pi$-bonds in rhenabenzene exhibit very little participation from the Re 5d orbitals (Figure 4d). Hence, the $\pi$-bonding in $ReB_6^-$ is even more similar to that of benzene than that of rhenabenzene, and $ReB_6^-$ can be considered as a true metallaboron analog of metallabenzenes. It should be pointed out that planar metallacycles can exhibit both Hückel and Möbius aromaticity because of the possible participation of the $d_{xz}$ orbital in the $\pi$-bonding.[71,72] Möbius aromaticity can occur for $4n$ $\pi$-metallacycles, such as the seven-membered ring metalla-cycloheptatriene [$8\pi$, $FeH_2(CH)_6$].[71,72] The $ReB_6^-$ cluster is clearly a Hückel aromatic system. It is conceivable that larger planar $ReB_n^-$ clusters may display Möbius aromaticity.

To further characterize the aromaticity in $ReB_6^-$, its NICS values were computed and compared with those of benzene and $B_{19}^-$ (ref 36) in Table S3 (SI). For $ReB_6^-$, since the central boron atom is very close to the geometric center of the molecule, we also computed the NICS values at different sites besides the geometric center (Table S3, SI). The large negative NICS values within the plane of the cluster in sites A, B, and C suggest strong $\sigma$-aromaticity. The $NICS_{zz}$ values for $ReB_6^-$ are all negative when the distance above the molecular plane is smaller than 0.6 Å, indicating strong $\pi$-aromaticity. The $NICS_{zz}$ value is very negative at site A, while less negative at site C. The values become more positive as the distance increases and the $NICS_{zz}(1)$ at site X above the central B atom is +4.22. A positive $NICS_{zz}$ value was also found for the doubly aromatic $B_{19}^-$ cluster at 0.2 Å above the plane (Table S3, SI), which features a boron atom at the geometric center.[36] Overall, the mainly negative $NICS_{zz}$ values are consistent with the AdNDP results that $ReB_6^-$ possesses both $\sigma$- and $\pi$-aromaticity and can be considered as a true metallaboron analog of metallabenzenes.

## CONCLUSIONS

We have produced the $ReB_6^-$ cluster and investigated its structure and bonding using high-resolution photoelectron imaging and computational chemistry. High-resolution photoelectron imaging for $AlB_6^-$ has also been done for comparison. Accurate electron affinities are measured for $ReB_6$ and $AlB_6$, as well as their vibrational frequencies. The $ReB_6^-$ cluster is found to have a planar B-centered hexagonal structure with $C_{2v}$ symmetry and a closed-shell electronic structure. Chemical bonding analyses revealed that $ReB_6^-$ possess three delocalized $\sigma$-bonds and three delocalized $\pi$-bonds, rendering it doubly aromatic. In comparison, the $AlB_6^-$ cluster has three delocalized $\sigma$-bonds, but only two delocalized $\pi$-bonds. Thus, it is $\pi$-antiaromatic, consistent with its out-of-plane distortion, analogous to that in the prototypical antiaromatic cyclooctatetraene ($C_8H_8$). The delocalized $\pi$-bonding in $ReB_6^-$ is compared with that in both benzene and rhenabenzene [$(CO)_4ReC_5H_5$]. The $\pi$-bonding in $ReB_6^-$ is found to be similar to that in benzene with the Re 5d orbitals participating in the delocalized bonding. Hence, $ReB_6^-$ can be considered as a metallaboron analog of the metallabenzenes. The current study suggests that other metallaboron analogs of metallabenzenes should exist and that these species may be viable for bulk syntheses with suitable ligation of the metal site.

## ASSOCIATED CONTENT

### Supporting Information

The Supporting Information is available free of charge on the ACS Publications website at DOI: 10.1021/jacs.9b09110.

Computed vibrational frequencies, molecular orbitals, Franck−Condon simulations, displacement vectors of


DOI: 10.1021/jacs.9b09110
J. Am. Chem. Soc. 2019, 141, 17854−17860

vibrational modes, and full AdNDP analyses for $ReB_6^-$ and $AlB_6^-$ (PDF)

## ■ AUTHOR INFORMATION


### Corresponding Author

* lai-sheng_wang@brown.edu

### ORCID

Lai-Sheng Wang: 0000-0003-1816-5738


### Notes

The authors declare no competing financial interest.

## ■ ACKNOWLEDGMENTS

This work was supported by the National Science Foundation (Grant CHE-1763380). G.S.K. was supported by a Philip A. Smith Chemistry Fellowship.

## ■ REFERENCES


(1) Thorn, D. L.; Hoffmann, R. Delocalization in Metallocycles. *Nouv. J. Chim.* **1979**, *3*, 39−45.

(2) Bleeke, J. R. Metallabenzenes. *Chem. Rev.* **2001**, *101*, 1205−1228.

(3) Frogley, B. J.; Wright, L. J. Recent Advances in Metallaaromatic Chemistry. *Chem. - Eur. J.* **2018**, *24*, 2025−2038.

(4) Fernández, I.; Frenking, G.; Merino, G. Aromaticity of Metallabenzenes and Related Compounds. *Chem. Soc. Rev.* **2015**, *44*, 6452−6463.

(5) Elliott, G. P.; Roper, W. R.; Waters, J. M. Metallacyclohexatrienes or 'Metallabenzenes.' Synthesis of Osmabenzene Derivatives and *X*-ray Crystal Structure of [Os(CSCHCHCHCH)(CO)($PPh_3$)$_2$]. *J. Chem. Soc., Chem. Commun.* **1982**, 811−813.

(6) Rickard, C. E. F.; Roper, W. R.; Woodgate, S. D.; Wright, L. J. Electrophilic Aromatic Substitution Reactions of a Metallabenzene: Nitration and Halogenation of the Osmabenzene [Os{C(SMe)-CHCHCHCH}I(CO)($PPh_3$)$_2$]. *Angew. Chem., Int. Ed.* **2000**, *39*, 750−752.

(7) Hung, W. Y.; Zhu, J.; Wen, T. B.; Yu, K. P.; Sung, H. H. Y.; Williams, I. D.; Lin, Z.; Jia, G. Osmabenzenes from the Reactions of a Dicationic Osmabenzyne Complex. *J. Am. Chem. Soc.* **2006**, *128*, 13742−13752.

(8) Bleeke, J. R.; Behm, R.; Xie, Y. F.; Chiang, M. Y.; Robinson, K. D.; Beatty, A. M. Synthesis, Structure, Spectroscopy, and Reactivity of a Metallabenzene. *Organometallics* **1997**, *16*, 606−623.

(9) Paneque, M.; Posadas, C. M.; Poveda, M. L.; Rendón, N.; Salazar, V.; Oñate, E.; Mereiter, K. Formation of Unusual Iridabenzene and Metallanaphthalene Containing Electron-Withdrawing Substituents. *J. Am. Chem. Soc.* **2003**, *125*, 9898−9899.

(10) Jacob, V.; Weakley, T. J. R.; Haley, M. M. Metallabenzenes and Valence Isomers. Synthesis and Characterization of a Platinabenzene. *Angew. Chem., Int. Ed.* **2002**, *41*, 3470−3473.

(11) Yang, J.; Jones, W. M.; Dixon, J. K.; Allison, N. T. Detection of a Ruthenabenzene, Ruthenaphenoxide, and Ruthenaphenanthrene Oxide: The First Metalla Aromatics of a Second-Row Transition Metal. *J. Am. Chem. Soc.* **1995**, *117*, 9776−9777.

(12) Zhang, H.; Xia, H.; He, G.; Wen, T. B.; Gong, L.; Jia, G. Synthesis and Characterization of Stable Ruthenabenzenes. *Angew. Chem., Int. Ed.* **2006**, *45*, 2920−2923.

(13) Poon, K. C.; Liu, L.; Guo, T.; Li, J.; Sung, H. H. Y.; Williams, I. D.; Lin, Z.; Jia, G. Synthesis and Characterization of Rhenabenzenes. *Angew. Chem., Int. Ed.* **2010**, *49*, 2759−2762.

(14) Lin, R.; Lee, K. H.; Poon, K. C.; Sung, H. H. Y.; Williams, I. D.; Lin, Z.; Jia, G. Synthesis of Rhenabenzenes from the Reactions of Rhenacyclobutadienes with Ethoxyethyne. *Chem. - Eur. J.* **2014**, *20*, 14885−14899.

(15) Wang, T.; Li, S.; Zhang, H.; Lin, R.; Han, F.; Lin, Y.; Wen, T. B.; Xia, H. Annulation of Metallabenzenes: From Osmabenzene to Osmabenzothiazole to Osmabenzoxazole. *Angew. Chem., Int. Ed.* **2009**, *48*, 6453−6456.

(16) Gilbertson, R. D.; Lau, T. L. S.; Lanza, S.; Wu, H. P.; Weakley, T. J. R.; Haley, M. M. Synthesis, Spectroscopy, and Structure of a Family of Iridabenzenes Generated by the Reaction of Vaska-Type Complexes with a Nucleophilic 3-Vinyl-1-cyclopropene. *Organometallics* **2003**, *22*, 3279−3289.

(17) Zhu, J.; Jia, G.; Lin, Z. Understanding Nonplanarity in Metallabenzene Complexes. *Organometallics* **2007**, *26*, 1986−1995.

(18) Chen, Z. N.; Fu, G.; Zhang, I. Y.; Xu, X. Understanding the Nonplanarity in Aromatic Metallabenzenes: A $\sigma$-Control Mechanism. *Inorg. Chem.* **2018**, *57*, 9205−9214.

(19) Lipscomb, W. N. The Boranes and Their Relatives. *Science* **1977**, *196*, 1047−1055.

(20) Aihara, J.-i. Three-Dimensional Aromaticity of Polyhedral Boranes. *J. Am. Chem. Soc.* **1978**, *100*, 3339−3342.

(21) Schleyer, P. v. R.; Najafian, K. Stability and Three-Dimensional Aromaticity of *Closo*-Monocarbaborane Anions, $CB_{n-1}H_n^-$, and *Closo*-Dicarboranes, $C_2B_{n-2}H_n$. *Inorg. Chem.* **1998**, *37*, 3454−3470.

(22) Schleyer, P. v. R.; Najafian, K.; Mebel, A. M. The Large *Closo*-Borane Dianions, $B_nH_n^{2-}$ ($n$ = 13−17) Are Aromatic, Why Are They Unknown? *Inorg. Chem.* **1998**, *37*, 6765−6772.

(23) Poater, J.; Solà, M.; Viñas, C.; Teixidor, F. $\pi$ Aromaticity and Three-Dimensional Aromaticity: Two sides of the Same Coin? *Angew. Chem., Int. Ed.* **2014**, *53*, 12191−12195.

(24) Zhai, H. J.; Kiran, B.; Li, J.; Wang, L. S. Hydrocarbon Analogs of Boron Clusters: Planarity, Aromaticity, and Antiaromaticity. *Nat. Mater.* **2003**, *2*, 827−833.

(25) Zhai, H. J.; Alexandrova, A. N.; Birch, K. A.; Boldyrev, A. I.; Wang, L. S. Hepta- and Octa-Coordinated Boron in Molecular Wheels of 8- and 9-Atom Boron Clusters: Observation and Confirmation. *Angew. Chem., Int. Ed.* **2003**, *42*, 6004−6008.

(26) Alexandrova, A. N.; Boldyrev, A. I.; Zhai, H. J.; Wang, L. S. All-Boron Aromatic Clusters as Potential New Inorganic Ligands and Building Blocks in Chemistry. *Coord. Chem. Rev.* **2006**, *250*, 2811−2866.

(27) Zubarev, D. Y.; Boldyrev, A. I. Comprehensive Analysis of Chemical Bonding in Boron Clusters. *J. Comput. Chem.* **2007**, *28*, 251−268.

(28) Sergeeva, A. P.; Popov, I. A.; Piazza, Z. A.; Li, W. L.; Romanescu, C.; Wang, L. S.; Boldyrev, A. I. Understanding Boron through Size-Selected Clusters: Structure, Chemical Bonding, and Fluxionality. *Acc. Chem. Res.* **2014**, *47*, 1349−1358.

(29) Boldyrev, A. I.; Wang, L. S. Beyond Organic Chemistry: Aromaticity in Atomic Clusters. *Phys. Chem. Chem. Phys.* **2016**, *18*, 11589−11605.

(30) Mercero, J. M.; Boldyrev, A. I.; Merino, G.; Ugalde, J. M. Recent Developments and Future Prospects of All-Metal Aromatic Compounds. *Chem. Soc. Rev.* **2015**, *44*, 6519−6534.

(31) Pan, S.; Barroso, J.; Jalife, S.; Heine, T.; Asmis, K. R.; Merino, G. Fluxional Boron Clusters: From Theory to Reality. *Acc. Chem. Res.* **2019**, *52*, 2732−2744.

(32) Zhai, H. J.; Wang, L. S.; Alexandrova, A. N.; Boldyrev, A. I. On the Electronic Structure and Chemical Bonding of $B_5^-$ and $B_5$ by Photoelectron Spectroscopy and *Ab Initio* Calculations. *J. Chem. Phys.* **2002**, *117*, 7917−7924.

(33) Alexandrova, A. N.; Boldyrev, A. I.; Zhai, H. J.; Wang, L. S.; Steiner, E.; Fowler, P. W. Structure and Bonding in $B_6^-$ and $B_6$: Planarity and Antiaromaticity. *J. Phys. Chem. A* **2003**, *107*, 1359−1369.

(34) Alexandrova, A. N.; Boldyrev, A. I.; Zhai, H. J.; Wang, L. S. Electronic Structure, Isomerism, and Chemical Bonding in $B_7^-$ and $B_7$. *J. Phys. Chem. A* **2004**, *108*, 3509−3517.

(35) Sergeeva, A. P.; Zubarev, D. Y.; Zhai, H. J.; Boldyrev, A. I.; Wang, L. S. A Photoelectron Spectroscopic and Theoretical Study of $B_{16}^-$ and $B_{16}^{2-}$: An All-Boron Naphthalene. *J. Am. Chem. Soc.* **2008**, *130*, 7244−7246.




DOI: 10.1021/jacs.9b09110
J. Am. Chem. Soc. 2019, 141, 17854−17860

(36) Huang, W.; Sergeeva, A. P.; Zhai, H. J.; Averkiev, B. B.; Wang, L. S.; Boldyrev, A. I. A Concentric Planar Doubly π Aromatic $B_{19}^-$ Cluster. *Nat. Chem.* **2010**, *2*, 202−206.
(37) Sergeeva, A. P.; Piazza, Z. A.; Romanescu, C.; Li, W. L.; Boldyrev, A. I.; Wang, L. S. $B_{22}^-$ and $B_{23}^-$: All-Boron Analogues of Anthracene and Phenanthrene. *J. Am. Chem. Soc.* **2012**, *134*, 18065−18073.
(38) Piazza, Z. A.; Hu, H. S.; Li, W. L.; Zhao, Y. F.; Li, J.; Wang, L. S. Planar Hexagonal $B_{36}$ As A Potential Basis for Extended Single-Atom Layer Boron Sheets. *Nat. Commun.* **2014**, *5*, 3113.
(39) Wang, L. S. Photoelectron Spectroscopy of Size-Selected Boron Clusters: From Planar Structures to Borophenes and Borospherenes. *Int. Rev. Phys. Chem.* **2016**, *35*, 69−142.
(40) Zubarev, D. Y.; Boldyrev, A. I. Developing Paradigms of Chemical Bonding: Adaptive Natural Density Partitioning. *Phys. Chem. Chem. Phys.* **2008**, *10*, 5207−5217.
(41) Romanescu, C.; Sergeeva, A. P.; Li, W. L.; Boldyrev, A. I.; Wang, L. S. Planarization of $B_7^-$ and $B_{12}^-$ Clusters by Isoelectronic Substitution: $AlB_6^-$ and $AlB_{11}^-$. *J. Am. Chem. Soc.* **2011**, *133*, 8646−8653.
(42) Exner, K.; Schleyer, P. v. R. Planar Hexacoordinate Carbon: A Viable Possibility. *Science* **2000**, *290*, 1937−1940.
(43) Wang, Z. X.; Schleyer, P. v. R. Construction Principles of "Hyparenes": Families of Molecules with Planar Pentacoordinate Carbons. *Science* **2001**, *292*, 2465−2469.
(44) Alexandrova, A. N.; Boldyrev, A. I.; Zhai, H. J.; Wang, L. S. Photoelectron Spectroscopy and Ab Initio Study of the Doubly-Antiaromatic $B_6^{2-}$ Dianion in the $LiB_6^-$ Cluster. *J. Chem. Phys.* **2005**, *122*, 054313.
(45) Wang, L. M.; Huang, W.; Averkiev, B. B.; Boldyrev, A. I.; Wang, L. S. $CB_7^-$: Experimental and Theoretical Evidence Against Hypercoordinated Planar Carbon. *Angew. Chem., Int. Ed.* **2007**, *46*, 4550−4553.
(46) Averkiev, B. B.; Zubarev, D. Y.; Wang, L. M.; Huang, W.; Wang, L. S.; Boldyrev, A. I. Carbon Avoids Hyper Coordination in $CB_6^-$, $CB_6^{2-}$, and $C_2B_5^-$ Planar Carbon-Boron Clusters. *J. Am. Chem. Soc.* **2008**, *130*, 9248−9250.
(47) Chen, Q.; Zhai, H. J.; Li, S. D.; Wang, L. S. On the Structures and Bonding in Boron-Gold Alloy Clusters: $B_6Au_n^-$ and $B_6Au_n$ ($n$ = 1−3). *J. Chem. Phys.* **2013**, *138*, 084306.
(48) Li, W. L.; Ivanov, A. S.; Federič, J.; Romanescu, C.; Černušák, I.; Boldyrev, A. I.; Wang, L. S. On the Way to the Highest Coordination Number in the Planar Metal-Centred Aromatic $Ta©B_{10}^-$ Cluster: Evolution of the Structures of $TaB_n^-$ ($n$ = 3 − 8). *J. Chem. Phys.* **2013**, *139*, 104312.
(49) Robinson, P. J.; Zhang, X.; McQueen, T.; Bowen, K. H.; Alexandrova, A. N. $SmB_6^-$ Cluster Anion: Covalency Involving f Orbitals. *J. Phys. Chem. A* **2017**, *121*, 1849−1854.
(50) Mason, J. L.; Harb, H.; Huizenga, C. D.; Ewigleben, J. C.; Topolski, J. E.; Hratchian, H. P.; Jarrold, C. C. Electronic and Molecular Structures of the $CeB_6$ Monomer. *J. Phys. Chem. A* **2019**, *123*, 2040−2048.
(51) León, I.; Yang, Z.; Liu, H. T.; Wang, L. S. The Design and Construction of A High-Resolution Velocity-Map Imaging Apparatus for Photoelectron Spectroscopy Studies of Size-Selected Clusters. *Rev. Sci. Instrum.* **2014**, *85*, 083106.
(52) Dick, B. Inverting Ion Images without Abel Inversion: Maximum Entropy Reconstruction of Velocity Maps. *Phys. Chem. Chem. Phys.* **2014**, *16*, 570−580.
(53) Clark, J.; Call, S. T.; Austin, D. E.; Hansen, J. C. Computational Study of Isoprene Hydroxyalkyl Peroxy Radical−Water Complexes ($C_5H_8(OH)O_2$−$H_2O$). *J. Phys. Chem. A* **2010**, *114*, 6534−6541.
(54) Averkiev, B. B.; Call, S.; Boldyrev, A. I.; Wang, L. M.; Huang, W.; Wang, L. S. Photoelectron Spectroscopy and Ab Initio Study of the Structure and Bonding of $Al_7N^-$ and $Al_7N$. *J. Phys. Chem. A* **2008**, *112*, 1873−1897.
(55) Call, S. T.; Zubarev, D. Y.; Boldyrev, A. I. Global Minimum Structure Searches via Particle Swarm Optimization. *J. Comput. Chem.* **2007**, *28*, 1177−1186.
(56) Kirkpatrick, S.; Gelatt, C. D., Jr.; Vecchi, M. P. Optimization by Simulated Annealing. *Science* **1983**, *220*, 671−680.
(57) Perdew, J. P.; Burke, K.; Ernzerhof, M. Generalized Gradient Approximation Made Simple. *Phys. Rev. Lett.* **1996**, *77*, 3865−3868.
(58) Hay, P. J.; Wadt, W. R. Ab Initio Effective Core Potentials for Molecular Calculations. Potentials for the Transition Metal Atoms Sc to Hg. *J. Chem. Phys.* **1985**, *82*, 270−283.
(59) Becke, A. D. Density-Functional Thermochemistry. III. The Role of Exact Exchange. *J. Chem. Phys.* **1993**, *98*, 5648−5652.
(60) Kendall, R. A.; Dunning, T. H., Jr.; Harrison, R. J. Electron Affinities of the First-Row Atoms Revisited. Systematic Basis Sets and Wave Functions. *J. Chem. Phys.* **1992**, *96*, 6796−6806.
(61) Figgen, D.; Peterson, K. A.; Dolg, M.; Stoll, H. Energy-Consistent Pseudopotentials and Correlation Consistent Basis Sets for the 5d Elements Hf-Pt. *J. Chem. Phys.* **2009**, *130*, 164108.
(62) Woon, D. E.; Dunning, T. H. Gaussian Basis Sets for Use in Correlated Molecular Calculations. III. The Atoms Aluminum through Argon. *J. Chem. Phys.* **1993**, *98*, 1358−1371.
(63) Schleyer, P. v. R.; Maerker, C.; Dransfeld, A.; Jiao, H.; van Eikema Hommes, N. J. R. Nucleus-Independent Chemical Shifts: A Simple and Efficient Aromaticity Probe. *J. Am. Chem. Soc.* **1996**, *118*, 6317−6318.
(64) Ervin, K. M.; Ramond, T. M.; Davico, G. E.; Schwartz, R. L.; Casey, S. M.; Lineberger, W. C. Naphthyl Radical: Negative Ion Photoelectron Spectroscopy, Franck−Condon Simulation, and Thermochemistry. *J. Phys. Chem. A* **2001**, *105*, 10822−10831.
(65) Frisch, M. J.; Trucks, G. W.; Schlegel, H. B.; Scuseria, G. E.; Robb, M. A.; Cheeseman, J. R.; Scalmani, G.; Barone, V.; Mennucci, B.; Petersson, G. A.; Nakatsuji, H.; Caricato, M.; Li, X.; Hratchian, H. P.; Izmaylov, A. F.; Bloino, J.; Zheng, G.; Sonnenberg, J. L.; Hada, M.; Ehara, M.; Toyota, K.; Fukuda, R.; Hasegawa, J.; Ishida, M.; Nakajima, T.; Honda, Y.; Kitao, O.; Nakai, H.; Vreven, T.; Montgomery, J. A., Jr.; Peralta, J. E.; Ogliaro, F.; Bearpark, M.; Heyd, J. J.; Brothers, E.; Kudin, K. N.; Staroverov, V. N.; Kobayashi, R.; Normand, J.; Raghavachari, K.; Rendell, A.; Burant, J. C.; Iyengar, S. S.; Tomasi, J.; Cossi, M.; Rega, N.; Millam, J. M.; Klene, M.; Knox, J. E.; Cross, J. B.; Bakken, V.; Adamo, C.; Jaramillo, J.; Gomperts, R.; Stratmann, R. E.; Yazyev, O.; Austin, A. J.; Cammi, R.; Pomelli, C. J.; Ochterski, W.; Martin, R. L.; Morokuma, K.; Zakrzewski, V. G.; Voth, G. A.; Salvador, P.; Dannenberg, J. J.; Dapprich, S.; Daniels, A. D.; Farkas, O.; Foresman, J. B.; Ortiz, J. V.; Cioslowski, J. *Gaussian 09*, Revision C.01; Gaussian, Inc.: Wallingford, CT, 2009.
(66) Romanescu, C.; Galeev, T. R.; Li, W. L.; Boldyrev, A. I.; Wang, L. S. Aromatic Metal-Centered Monocyclic Boron Rings: $Co©B_8^-$ and $Ru©B_9^-$. *Angew. Chem., Int. Ed.* **2011**, *50*, 9334−9337.
(67) Romanescu, C.; Galeev, T. R.; Li, W. L.; Boldyrev, A. I.; Wang, L. S. Geometric and Electronic Factors in the Rational Design of Transition-Metal-Centered Boron Molecular Wheels. *J. Chem. Phys.* **2013**, *138*, 134315.
(68) Romanescu, C.; Galeev, T. R.; Li, W. L.; Boldyrev, A. I.; Wang, L. S. Transition-Metal-Centered Monocyclic Boron Wheel Clusters ($M©B_n$): A New Class of Aromatic Borometallic Compounds. *Acc. Chem. Res.* **2013**, *46*, 350−358.
(69) Chen, T. T.; Li, W. L.; Bai, H.; Chen, W. J.; Dong, X. R.; Li, J.; Wang, L. S. $Re©B_8^-$ and $Re©B_9^-$: New Members of the Transition-Metal-Centered Borometallic Molecular Wheel Family. *J. Phys. Chem. A* **2019**, *123*, 5317−5324.
(70) Jian, T.; Cheung, L. F.; Czekner, J.; Chen, T. T.; Lopez, G. V.; Li, W. L.; Wang, L. S. $Nb_2©Au_6$: A Molecular Wheel with a Short Nb≡Nb Triple Bond Coordinated by an $Au_6$ Ring and Reinforced by sigma Aromaticity. *Chem. Sci.* **2017**, *8*, 7528−7536.
(71) Mauksch, M.; Tsogoeva, S. B. Strict Correlation of HOMO Topology and Magnetic Aromaticity Indices in d-Block Metalloaromatics. *Chem. - Eur. J.* **2018**, *24*, 10059−10063.
(72) Szczepanik, D. W.; Solà, M. Electron Delocalization in Planar Metallacycles: Hückel or Möbius Aromatic? *ChemistryOpen* **2019**, *8*, 219−227.


DOI: 10.1021/jacs.9b09110
*J. Am. Chem. Soc.* 2019, 141, 17854−17860